Nonlinear optics on deuterated silicon-rich nitride devices

Dawn T. H. Tan [a,b,*], Xavier X. Chia[a], Hongwei Gao[a], George F. R. Chen[a] and Doris K. T. Ng[b]
[a]Photonics Devices and System Group, Singapore University of Technology and Design, 8 Somapah Rd, Singapore 487372, Singapore
[b]Institute of Microelectronics (IME), Agency for Science, Technology and Research (A*STAR), 2 Fusionopolis Way, Innovis #08-02, Singapore 138634, Singapore
[*]*dawn_tan@sutd.edu.sg*

ABSTRACT

Silicon-rich nitride (SRN) devices provide higher optical nonlinearity than stoichiometric silicon nitride. Their growth using CMOS-compatible chemical vapor deposition allows their composition to be tunable. Conventional SRN typically utilizes silane gas which introduces absorption overtones at the 1.55μm wavelength region. As is also the case with stoichiometric silicon nitride, high temperature annealing can be used to reduce Si-H based absorption. An alternate approach towards eliminating Si-H absorption is by replacing silane gas with deuterated silane. The substitution of Si-H with Si-D induces a blue shift in the wavenumber of the bond absorption, thus removing the absorption overtone at the telecommunications region. Consequently, deuterated SRN provides lower material losses compared to non-deuterated SRN, while providing a design degree of freedom for tailoring its linear and nonlinear refractive indices. We present the material properties for deuterated SRN and its application towards linear and nonlinear photonic devices. We demonstrate improved device losses when deuterated SRN is used compared to non-deuterated SRN. We further quantify the optical properties and nonlinearity of grown films and demonstrate low power parametric wavelength conversion in deuterated SRN ring resonators.

Keywords: Nonlinear integrated optics, silicon rich nitride, deuterated silicon rich nitride.

1. INTRODUCTION

Silicon photonics is a core technology in a variety of areas including optical transceivers, optical sensors, quantum information processing and topological photonics [1-4]. It has evolved tremendously over the years, with initial research effort focused on crystalline silicon on insulator-based photonics, driven largely by its compatibility with complementary metal-oxide semiconductor (CMOS) processing and ease of integration with CMOS electronics. Crystalline silicon's nonlinear properties at telecommunications wavelengths suffer from some limitations, primarily from its 1.1eV indirect bandgap which results in deleterious two-photon and free-carrier absorption [5]. As these limitations were uncovered, research into stoichiometric silicon nitride-based photonics burgeoned. While its nonlinearity was 100X smaller than crystalline silicon, it had a larger bandgap to circumvent nonlinear losses. Consequently, silicon nitride saw extensive use in frequency comb-based applications including multi-wavelength sources and frequency synthesizers, as well as amplifiers. The ultra-low losses achieved in SiN typically required multi-step deposition using low pressure chemical vapor deposition, followed by high temperature annealing at 1200°C to eliminate Si-H bond overtones which induces absorption at the 1.55μm wavelength region [6,7]. As the field progressed, researchers discovered that increasing the silicon content in silicon nitride could bring about higher optical nonlinearities [8-12]. Silicon-rich nitride devices could be grown using low temperature chemical vapor deposition, with optical nonlinearities in the films being 100X larger than in stoichiometric SiN. This development greatly facilitated the development of low power, two-photon free nonlinear photonic devices for use in Bragg soliton applications, high gain optical parametric amplifiers and high spectro-temporal compression systems. Similar to SiN, Si-H bonds which exist in SRN films lead to material absorption at the telecommunications wavelength region. Most recently, the development of SRN-based nonlinear devices has extended to exploration into the use of deuterated silane [13-15]. This approach avoids the need for high temperature annealing to remove Si-H bond-based absorption. The use of deuterated silane (SiD_4) replaces Si-H bonds with Si-D bonds, thus shifting the absorption from the 1.55μm region to the 2.1μm region. Compared to conventional SRN films, deuterated silane (referred to hereafter as SRN:D) devices possess lower material losses, yielding lower waveguide propagation losses and higher quality factor resonators. In this paper, we describe the development of SRN:D, their

material properties compared to conventional SRN. Experimental characterization of their nonlinear properties as well as low power parametric wavelength conversion are presented.

2. DEUTERATED SILICON-RICH NITRIDE MATERIAL CHARACTERIZATION

The fundamental vibrational absorption and third vibrational overtone for Si-H bonds are located at 2200cm^{-1} and 6600cm^{-1} respectively. The latter results in absorption at the 1.5μm wavelength region. The shift in absorption by replacing Si-H with Si-D may be further analyzed using the quantum harmonic oscillator model which describes vibrational bond energies [16]:

$$-\frac{h^2}{2m}\frac{d^2\psi}{dx^2}+\frac{1}{2}kx^2\psi = E\psi \tag{1}$$

Here, h is Planck's constant, Ψ is the wave function, x is the displacement from equilibrium and E is energy. Using the boundary conditions, $\Psi = 0$, $x = \pm\infty$, we arrive at an expression for the vibrational bond energy [16]:

$$E_v = h.(1/2\pi).(v + 1/2)\sqrt{k/m_1 + k/m_2} \tag{2}$$

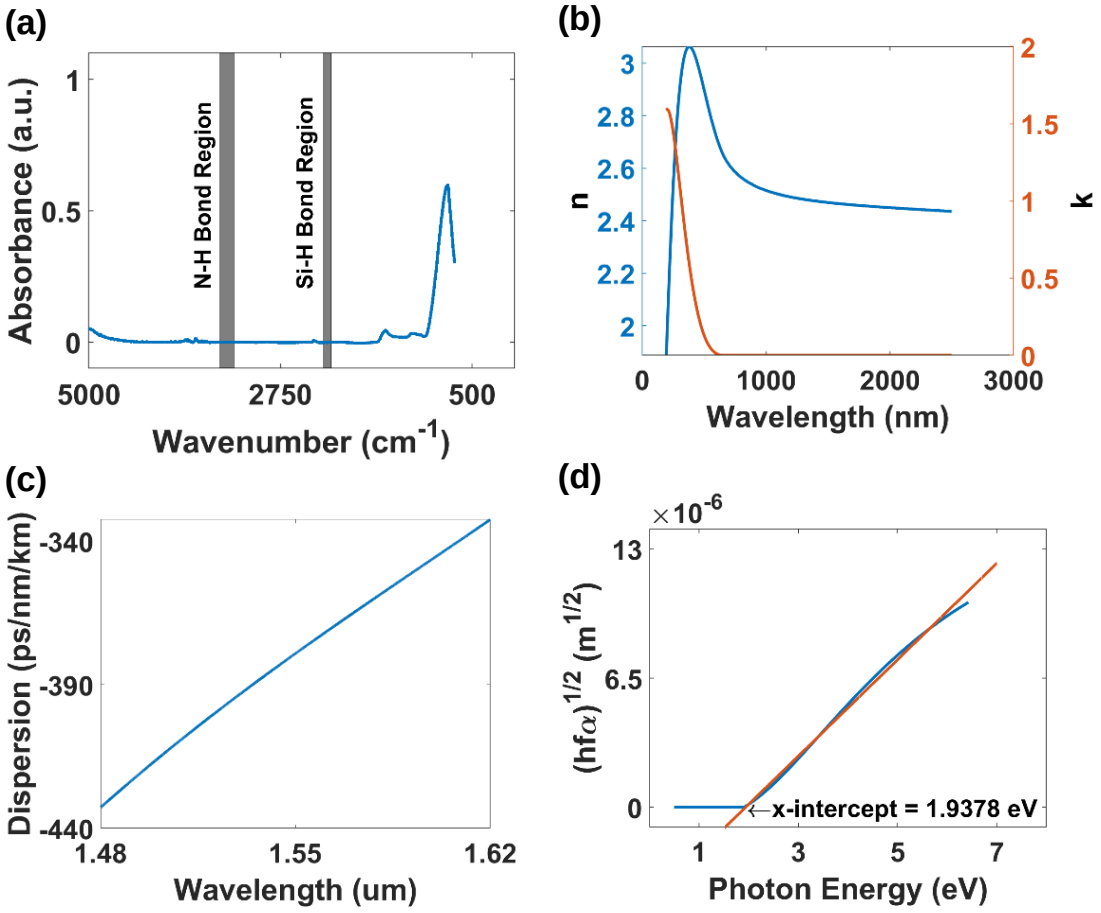

Fig. 1. (a) Baseline-adjusted absorbance plot exhibiting regions where Si-H and N-H bonds could occur. We note no peak occurrences in these regions, indicating absence or negligible Si-H and N-H bonds. (b) Refractive index n (—) and extinction coefficient k (—) data extracted using FTIR measurements (c) Material dispersion curves from 1480 nm-1620 nm for the SRN-D film (d) Tauc's plot of the SRN-D film with the original curve (—) and fitted line (—).

Here, υ is the vibrational quantum number (an integer), k is the bond's force constant and $m_{1,2}$ is the atomic mass for the two atoms making up the bond. The atomic mass for silicon (Si), deuterium (D) and hydrogen (H) is 28, 1 and 2 respectively. A change in m_1 or m_2 through the substitution of H with D will result changes the vibrational bond energy. From Eq. (2), it follows that the third vibrational overtone associated with Si-H at 6600 cm^{-1} (1.5 μm region) will decrease to 4670 cm^{-1} (2.1 μm region).

Fabrication of the deuterated SRN films is performed using plasma enhanced chemical vapor deposition. The deposition temperature of 350oC is significantly lower than that used in low pressure chemical vapor deposition (typically around 800^{o}C). Nitrogen gas is used in place of ammonia in order to suppress formation of N-H bonds. Deuterated silane gas (SiD_4) and N_2 gas with a flow rate ratio of 3:250 is used for the film growth. 310nm of SRN:D is deposited on a 5μm thermal oxide on silicon substrate. Film characterization is performed using Fourier-Transform Infrared (FTIR) spectroscopy. Figure 1 (a) shows the FTIR spectrum as well as the locations of typical absorption for the Si-H and N-H bonds could occur, at wavenumber range 2157 cm^{-1} to 2250 cm^{-1} and 3290 cm^{-1} to 3464 cm^{-1} respectively. No absorption peaks are observed in this region, indicating that there is minimal presence of Si-H and N-H bonds in the grown films [15].

The film's n and k as a function of wavelength is further extracted from the FTIR measurements. The linear refractive index at a wavelength of 1550nm is 2.46. It is further observed that the film exhibits normal dispersion at this wavelength. Next, Tauc's method is used to characterize the film's optical bandgap of 1.94eV. By plotting $(hf\alpha)^{\frac{1}{2}}$ vs hf, the x-intercept of the extrapolated linear segment provides the optical bandgap [17]. This value of optical bandgap translates to a wavelength of 640nm, which precludes two-photon absorption at 1550nm, an important property for efficient nonlinear optics.

3. NONLINEAR CHARACTERIZATION OF DEUTERATED SILICON-RICH NITRIDE DEVICES

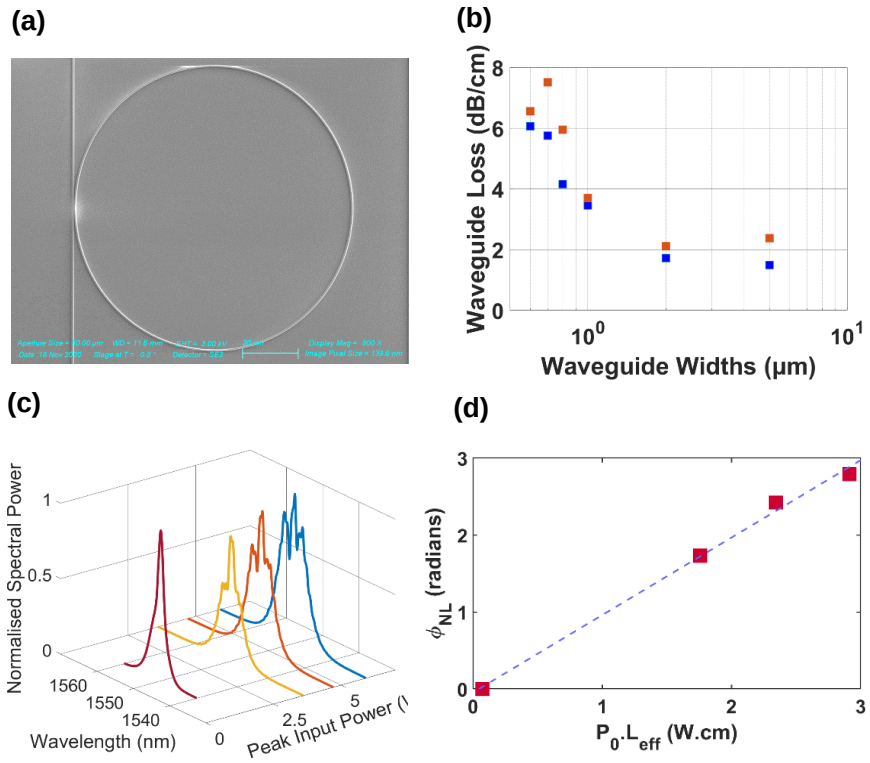

Fig. 2. (a) Scanning electron micrograph of a fabricated SRN:D microring resonator. (b) Waveguide propagation losses extracted from cutback measurements for the quasi-TE (■) and quasi-TM (■) modes. (c) Self-phase modulation spectra for peak input powers 3.6 W (—), 4.7 W (—), 5.9 W (—), and Source (—) (d) Modelled (···) and experimentally measured (—) SPM spectra for 1.3 pulses at a peak power, P_0 = 5.9 W. (d) Nonlinear phase shift (■) as a function of $P_0.L_{eff}$.

Fabrication of devices from the deposited SRN:D films is performed using electron-beam lithography, reactive ion etching and plasma enhanced chemical vapor deposition of 2 µm of SiO2 overcladding. We utilize a SRN:D thickness of 310 nm. Figure 2 (a) shows a scanning electron micrograph of a fabricated microring resonator. A comparison of propagation losses between the quasi-TE and quasi-TM modes is shown in Fig. 2 (b), where the TE modes have a lowest loss of 1.5dB/cm at a width of 5 µm. Self-phase modulation experiments using 1.3ps pulses was further performed in a 6.9mm waveguide with a cross section of 0.8 µm × 0.31 µm at a wavelength of 1.55 µm. Under these conditions, the calculated effective modal area A_{eff} was 0.42 µm^2. An analysis of the nonlinear phase shift as a function of $P_0.L_{\text{eff}}$, where P_0 and L_{eff} are the peak power and effective length respectively allows us to extract the nonlinear parameter to be 95 W^{-1}/m (Fig. 2 (d)) and a film Kerr nonlinearity of 9.8×10^{-18} m^{2}W^{-1}.

Figure 3 (a) shows the transmission spectrum of a SRN:D microring resonator with loaded and intrinsic quality factors of 99,000 and 135,000 respectively [16]. The impact of increasing the gap (decreasing the coupling) in the bus waveguide and ring on the microring resonator transmission spectrum is shown in Fig. 3 (b), where it can be observed that the extinction ratios decrease as the gap increases.

Using the fabricated microring resonators, we perform parametric wavelength conversion experiments. A continuous-wave pump and signal is combined using a 3dB coupler, adjusted for TE-mode prior to coupling into the microring resonator using tapered lensed fibers. Figure 4 shows the four-wave mixing spectra as a function of pump power and pump-signal resonance detuning, measured using an optical spectrum analyzer. Cascaded four-wave mixing may be observed in all spectra. Table 1 further lists the measured conversion efficiencies for the first and second idlers for each of the spectra shown in Fig. 4.

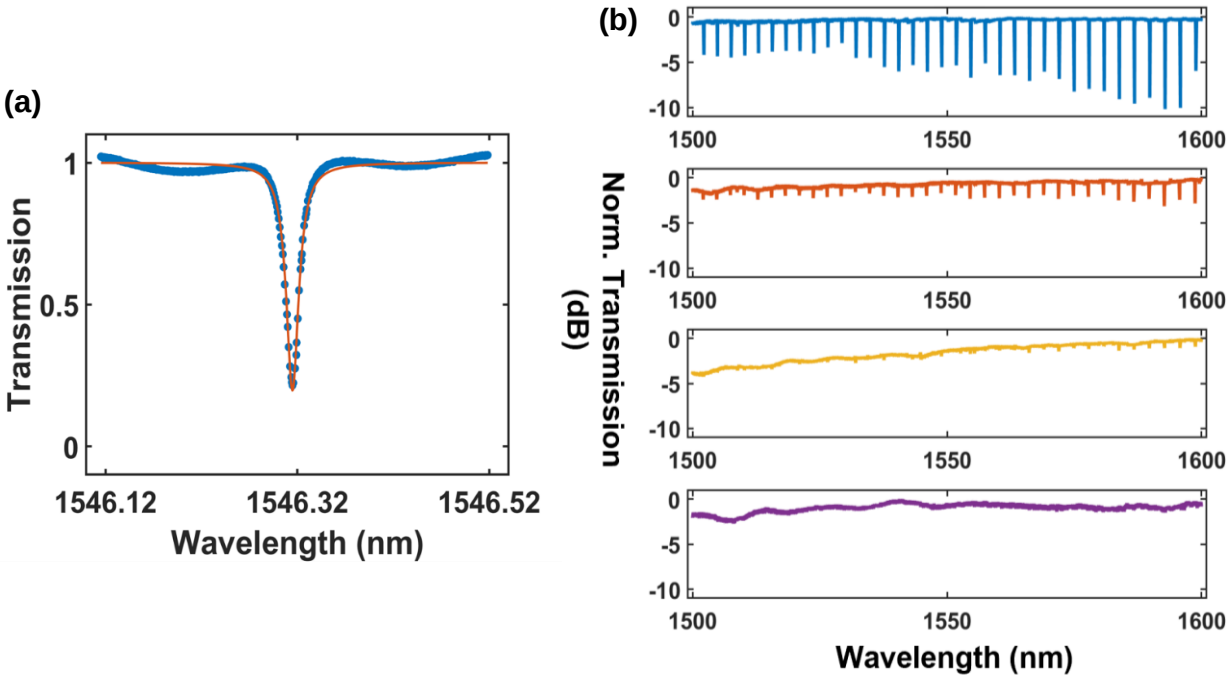

Fig. 3 (a) Measured transmission spectrum of a SRN:D microring resonator with resonator spectrum with loaded quality factor of 99,000 and intrinsic quality factor of 135,000. (b) Normalized transmission spectrum of microring resonators with gap widths 0.2 µm (—), 0.3µm (—), 0.4µm (—), and 0.5 µm (—) as a function of coupling ratios.

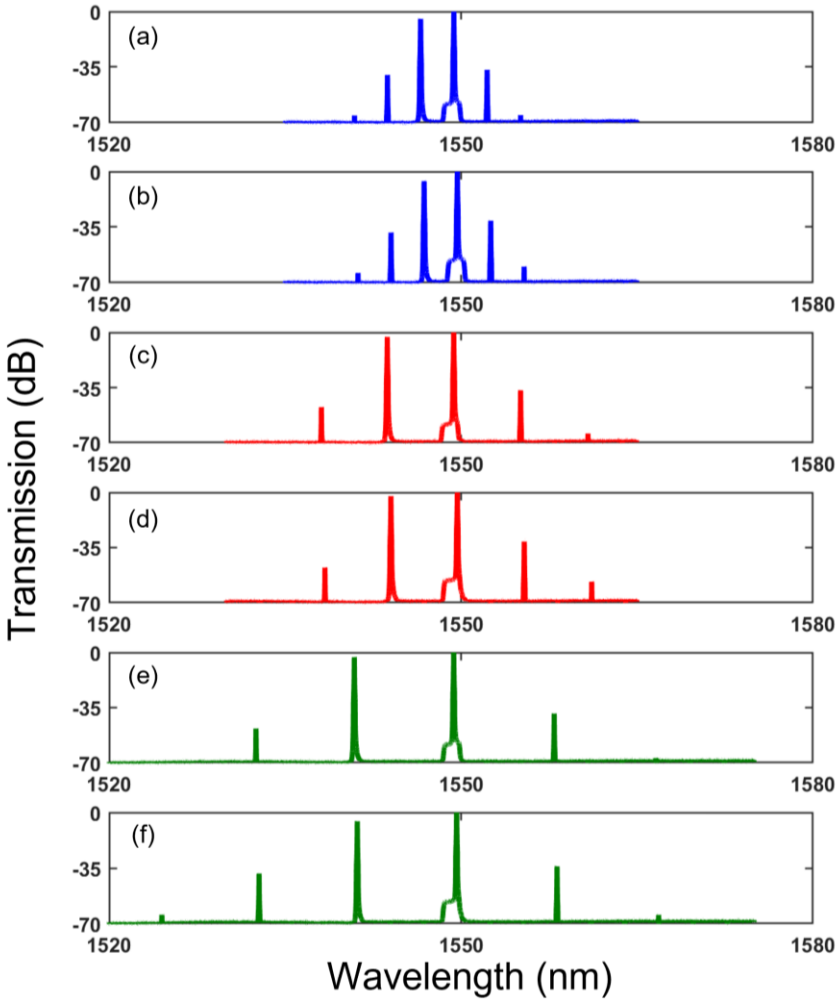

Fig. 4. Cascaded FWM plots with the signal source coupled into $\lambda_{s,1}$ (—) with (a) P_p = 10 mW and (b) P_p = 20 mW , $\lambda_{s,2}$ (—) with (c) P_p = 10 mW and (d) P_p = 20 mW, and $\lambda_{s,3}$ (—) with (e) P_p = 10 mW and (f) P_p = 17.5 mW . The slight red-shift of the output spectra with higher pump powers P_p is attributed to the high thermo-optic shift of the resonators since the sources have to be re-driven into the resonances. Table 2 shows the individual conversion efficiencies.

Resonance	Pump Power	1st Idler CE	2nd Idler CE
$\lambda_{s,1}$	10 mW	-36.2 dB	-64.8 dB
	20 mW	-30.1 dB	-59.0 dB
$\lambda_{s,2}$	10 mW	-35.9 dB	-63.4 dB
	20 mW	-30.4 dB	-55.9 dB
$\lambda_{s,3}$	10 mW	-38.2 dB	-66.4 dB
	17.5 mW	-32.9 dB	-60.5 dB

Table 1. Measured FWM Conversion efficiencies (CEs) for 1st and 2nd idlers.

4. CONCLUSIONS

Deuterated silicon-rich nitride provides an alternative to stoichiometric silicon which is TPA-free and FCA-free at telecommunications wavelengths. In addition, its film composition may be tailored using the precursor gas ratios during growth, thus allowing the linear and nonlinear optical properties to be tuned. Another key advantage to the demonstrated deuterated silicon-rich nitride devices is their low temperature and single step growth. The low thermal budget reduces the process complexity and facilitates its use in backend CMOS-processes.

The optical nonlinearity of the demonstrated SRN:D waveguides are almost 100X larger than in stoichiometric silicon nitride. Conversion efficiencies of -30dB and -59dB for the first and second idler are achieved at 20mW pump power. The SRN:D platform may be used advantageously in the future for the development of low power nonlinear photonic devices such as nonlinear Bragg gratings [18,19], optical parametric oscillators [20] and high gain amplifiers [21].

ACKNOWLEDGMENTS

Funding from the Quantum Engineering Programme 2.0 grant (NRF2022-QEP2-01-P08), Ministry of Education ACRF Tier 2 Grant (T2EP50121-0019), A*STAR MTC Grant (M21K2c0119) and A*STAR Institute of Microelectronics (C220415015) is gratefully acknowledged. The authors acknowledge processing and facilities under the National Research Foundation, Prime Minister's Office, Singapore, under its Medium Sized Centre Program, the Singapore University of Technology and Design, the UCSB Nanofabrication Facility, an open access laboratory, and the Agency for Science, Technology, and Research.

REFERENCES

[1] R. Nagarajan, I. Lyubomirsky, O. Agazzi, *J. Light. Technol.* 39, 16 (2021).
[2] R. Nagarajan, M. Filer, Y. Fu, M. Kato, T. Rope, J. Stewart, *J. Opt. Commun. Netw.*, 10, 7 (2018).
[3] J. Wang, F. Sciarrino, A. Laing, and M. G. Thompson, *Nat. Photonics* 14, 273–284 (2020).
[4] D. T. H. Tan, *Adv. Photonics Res*. 2: 2100010 (2021).
[5] H. K. Tsang, C. S. Wong, T. K. Liang, I. E. Day, S. W. Roberts, A. Harpin, J. Drake, and M. Asghari, *Appl. Phys. Lett*. 80, 416 (2002).
[6] X. Ji, Felippe A. S. Barbosa, S. P. Roberts, A. Dutt, J. Cardenas, Y. Okawachi, A. Bryant, A. L. Gaeta, and M. Lipson, *Optica* 4, 619-624 (2017)
[7] J. Liu, G. Huang, R. N. Wang, J. He, A. S. Raja, T. Liu, N. J. Engelsen and T. J. Kippenberg, *Nat Commun* 12, 2236 (2021).
[8] T. Wang, D. K. T. Ng, S.-K. Ng, Y.-T. Toh, A. K. L. Chee, G. F. R. Chen, Q. Wang, and D. T. H. Tan, *Laser & Photonics Reviews* **9**, 498-506 (2015).
[9] C.-L. Wu, Y.-H. Lin, S.-P. Su, B.-J. Huang, C.-T. Tsai, H.-Y. Wang, Y.-C. Chi, C.-I. Wu, and G.-R. Lin, *ACS Photonics* 2, 1141-1154 (2015).
[10] D. T. H. Tan, K. J. A. Ooi, and D. K. T. Ng, *Photon. Res.* **6**, B50-B66 (2018).
[11] C. J. Krückel, A. Fülöp, Z. Ye, P. A. Andrekson, and V. Torres-Company, *Opt. Express* **25**, 15370-15380 (2017).
[12] C. Lacava, S. Stankovic, A. Z Khokhar, T. Dominguez Bucio, F. Y. Gardes. G. T Reed, D. J Richardson and P. Petropoulos, *Scientific Reports*, 7(1), 22, (2017).
[13] X. X. Chia, G. F. R. Chen, Y. Cao, P. Xing, H. Gao, D. K. T. Ng and D. T. H. Tan, Sci. Rep. 12:12697 (2022).
[14] X. X. Chia, J. W. Choi, P. Xing, H. Gao, G. F. R. Chen, D. K. T. Ng and D. T. H. Tan, *Journal of Lightwave Technol.* 41(10),3115-3130 (2023).
[15] X. X. Chia and D. T. H. Tan, *Nanophotonics* 12(8), 1613-1631 (2023).
[16] P. W. Atkins and J. De Paula, *Physical chemistry* (Oxford University Press, Oxford, 2006).
[17] P. Makuła, M. Pacia, and W. Macyk, *The Journal of Physical Chemistry Letters* **9**, 6814-6817 (2018).
[18] J. W. Choi, B.-U. Sohn, E. Sahin, G. F. R. Chen, P. Xing, D. K. T. Ng, B. J. Eggleton and D. T. H. Tan, *Optica* 10, 1452-1460 (2023).
[19] D. T. H. Tan, B. J. Eggleton, *Laser Photonics Re*v 17, 2300373 (2023).
[20] P. Xing, G. F. R. Chen, H. Gao, X. X. Chia, A. M. Agarwal, L. C. Kimerling and D. T. H. Tan, *Nanophotonics*, 11(14), 3269-3280 (2022).
[21] K. J. A. Ooi, D. K. T. Ng, T. Wang, A. K. L. Chee, S. K. Ng, Q. Wang, L. K. Ang, A. M. Agarwal, L. C. Kimerling and D. T. H. Tan, *Nat. Commun*. 8, 13878 (2017).